CSIRO PUBLISHING

Environ. Chem.
https://doi.org/10.1071/EN17224

Research Paper

Swelling and aggregation of Leonardite upon pH change and Pb^{II} binding: an AFM study

Federico dos Reis Copello,[A] *Leonardo Lizarraga,*[B] *Silvia Orsetti*[C] *and Fernando V. Molina*[A,D]

[A]INQUIMAE, Instituto de Química Física de Materiales, Ambiente y Energía, and Departamento de Química Inorgánica, Analítica y Química Física, FCEN, UBA, Buenos Aires C1428EGA, Argentina.
[B]CIBION, Centro de Investigaciones en Bionanociencias, CONICET, Consejo Nacional de Investigaciones Científicas y Técnicas 'Elizabeth Jares Erijman', Buenos Aires C1425FQD, Argentina.
[C]Institut für Geowissenschaften, Zentrum für angewandte Geowissenschaften, Eberhard-Karls Universität Tübingen, Tübingen 72074, Germany.
[D]Corresponding author. Email: fmolina@qi.fcen.uba.ar

Environmental context. Natural organic materials, such as humic substances, play key roles in the binding and environmental fate of metals. We study the interaction of protons and metal ions with humic acids, and show changes to the mechanical properties of the particles and their capability to fix metal pollutants. The results will help refine current models of metal behaviour in the environment.

Abstract. The swelling and aggregation of Leonardite humic acid, due to acid–base and Pb^{II} binding interactions, was studied through atomic force microscopy (AFM) tapping mode measurements and correlated with potentiometric experiments. These experiments allowed determination of parameters for the non-ideal competitive adsorption (NICA)-elastic polyelectrolyte network (EPN) model, which predicts size and electrostatic potential changes. AFM observations showed growth of agglomerates at low pH values. Height distribution analysis allowed discrimination of single particles from agglomerates. The size of individual particles increased slightly with pH increase. Agglomeration was evaluated through the dispersity, which increased at pH < 5, concomitant with a decrease of the electrostatic repulsion and an increase of protonated carboxylic groups, thus the agglomeration is attributed to both factors. In the presence of Pb^{II}, agglomeration is observed to rise strongly with the increase in metal concentration, which is attributed to bridging of humic particles by Pb^{II} ions. The AFM ex situ results suggest consistency between NICA-EPN predictions and experimental behaviour.

Additional keywords: environmental colloids, metals, soil chemistry.

Received 5 December 2017, accepted 23 February 2018, published online 25 June 2018

Introduction

Humic substances (HS) are important components of natural organic matter (NOM) in groundwaters and soils, where they have fundamental roles in many environmental processes, such as nutrient availability for plants, pollutant metal retention and mobility, and soil structure, among several other important properties (Senesi and Loffredo 1998; Baldock and Nelson 1999). HS show colloidal behaviour and interact with other chemical species in the natural environment, including binding of protons and inorganic cations. This ability, in particular for binding heavy metals, has an important role in the fate of such pollutants in the environment.

HS have been show to have a soft and permeable nature, as deduced from electrophoretic mobilities by Duval et al. (2005). Their results are interpreted considering HS as permeable particles, with a pH-dependent hydrodynamic size which increases as pH decreases in most of the range, and (for some cases) departs from this behaviour at the low and high pH extremes. The fact that the size increases as pH decreases is explained in terms of molecular aggregation, being less important at high pH values due to intermolecular electrostatic repulsion. At the high pH range (9–11) a size increase is observed, attributed to electrostatically driven molecular expansion; that is, aggregation is prevented and the observed changes are due to molecular swelling caused by the increasing charge. At the low range (pH 4–5), the hydrodynamic radius levels or decreases slightly, which is interpreted as the aggregates becoming more compact due to increased hydrogen bonding. Humic aggregation has also been observed and discussed by several authors (Simpson et al. 2002; Wershaw 2004; Sutton and Sposito 2005; Baigorri et al. 2007; Chilom and Rice 2009).

An important tool in the observation of HS is atomic force microscopy (AFM). It has been employed by several authors in the study of NOM, including HS (Balnois et al. 1999;

Plaschke et al. 2002; Balnois and Wilkinson 2002; Gorham et al. 2007; Chen et al. 2007). AFM allows observation of the structures of macromolecules and particles deposited on surfaces down to the nanometer level. The use of the so-called 'tapping mode' technique allows reliable determination of the height of soft materials such as NOM particles, because it minimises the contact and lateral forces between the tip and sample (Zhong et al. 1993); measurements in directions parallel to the surface have lower resolution due to the effect of tip size and the soft nature of HS.

Modelling of metal sorption to HS has interested researchers for many years (Buffle et al. 1990; Tipping 1998; Gustafsson et al. 2003; Goldberg 2005; Molina 2013), because models adequately describing sorption are required for predictive purposes. Such models, similar to the case of minerals like oxides and clays, generally comprise chemical (intrinsic) and electrostatic contributions. Modelling results for the intrinsic contribution can be interpreted in terms of conditional affinity spectra (Puy et al. 2008, 2009; David et al. 2010). The most commonly used humic models, non-ideal competitive adsorption (NICA)–Donnan (ND) (Kinniburgh et al. 1996, 1999) and Windermere humic aqueous model (WHAM) (Tipping 1998), show good fitting and prediction ability for many cases examined so far. More recently, a new electrostatic model for HS, the elastic polyelectrolyte network (EPN) model was developed, which predicts swelling and shrinking of HS particles as the humic charge changes. This model has been described thoroughly in the literature (Orsetti et al. 2010, 2013; Montenegro et al. 2014). Here a brief account is included in the Supplementary Material for easy reference.

In a previous work (Orsetti et al. 2013), the binding of Pb^{II} to HS was studied by potentiometric titrations and fluorescence measurements, and the results interpreted with the NICA-EPN model. The model was found to describe well the metal binding, and combined with the spectroscopic results, suggested that initial metal binding (observed as strongly binding sites), corresponded to multidentate complexation to carboxylate groups, including binding between groups of different humic molecules, promoting aggregation. Further binding (observed as weakly binding sites) corresponded to single ligand groups. Analysing literature data with the NICA-EPN model (Montenegro et al. 2014), it is found that the model describes well the binding data, and predicts particle swelling as the pH increases, but shrinking upon metal binding, due to decreased net charge.

In this work, the size changes and aggregation of Leonardite humic acid (LHA), as affected by pH and interaction with Pb^{II}, are investigated through an ex situ AFM study, and the results interpreted in terms of the NICA-EPN model.

Materials and methods

Standard International Humic Substances Society (IHSS) Leonardite humic acid (LHA) was used in the present study. Its main characterisation parameters are given in the IHSS site (http://humic-substances.org/). Acid–base potentiometric titrations were performed following usual procedures (Milne et al. 1995) at 1 g L^{-1} concentration and different ionic strength (I) values in $NaClO_4$. Pb^{II}–humic potentiometric titrations also followed known procedures (Benedetti et al. 1995), with 2 g L^{-1} LHA at pH values of 4.0 and 5.5, and an ionic strength ($NaClO_4$) of 0.1 M. Experimental details are given in the Supplementary Material.

For AFM measurements, stock solutions were prepared by dissolving LHA in NaOH solutions (pH 10) to get a concentration of 100 mg L^{-1}. From these solutions working solutions of 20 mg L^{-1} were immediately prepared at different pH values (pH range 2–11), and an ionic strength of 0.01 M $NaClO_4$. For Pb^{II} binding experiments, solutions containing Pb $(NO_3)_2$ at concentrations between 5 and 50 μM, and otherwise identical to the above described were prepared. Muscovite mica discs grade V1 (Ted Pella) of 10 mm diameter were cleaved using a scotch tape and immediately introduced for 30 min in a baker containing 15 mL of the 20 mg L^{-1} LHA solution of the selected pH or Pb^{II} concentration. Discs were then rinsed and dried at ambient conditions. The sorption method used to prepare the sample gives a better defined observation of molecular species present in the LHA solution (Balnois and Wilkinson 2002). A Bruker Multimode 8 SPM (Santa Barbara, CMA, USA) and a NanoScope V Controller (Santa Barbara, CMA, USA) were used. The AFM images were acquired in tapping mode using silicon tips with a spring constant of 1–5 N m^{-1} and a resonance frequency in the range of 60–100 kHz. Areas of 4 μm × 4 μm (512 × 512 pixels) were scanned. In tapping mode, the cantilever, which has a sharp tip at its free end, is excited near its free resonance frequency. The oscillation amplitude is used as a feedback parameter to measure the surface topography (García and Pérez 2002).The images were analysed using *Gwyddion* version 2.46 software (Brno, Czech Republic). Experimental and image processing details are given in the Supplementary Material. The statistical functions analysed were the number-average mean particle height (Eqn 1):

$$h_N = \frac{\sum_i n_i h_i}{N} \quad (1)$$

where n_i is the number of particles with height h_i and N the total number of particles; the weight-average mean height (Eqn 2):

$$h_W = \frac{\sum_i n_i h_i^2}{\sum_i n_i h_i} \quad (2)$$

the normalised total height (Eqn 3):

$$H_j = \frac{n_j h_j}{\sum_i n_i h_i} \quad (3)$$

and the dispersity (also known as polydispersity index) (Eqn 4):

$$D = \frac{h_W}{h_N} \quad (4)$$

Results and discussion

Leonardite acid–base and Pb interactions

Fig. 1a shows the acid–base titration curves of LHA at different ionic strengths (I) along with the fitted curves to the NICA-EPN model. A very good agreement between experiment and model is found. The fitted parameters are collected in Table 1, compared with literature values interpreted with the ND model by Milne et al. (2001). The metal binding parameters found here show little or no agreement with the ND results. The fractions of carboxylic and phenolic sites found in this work, and the corresponding log K_H values, are in reasonable agreement with

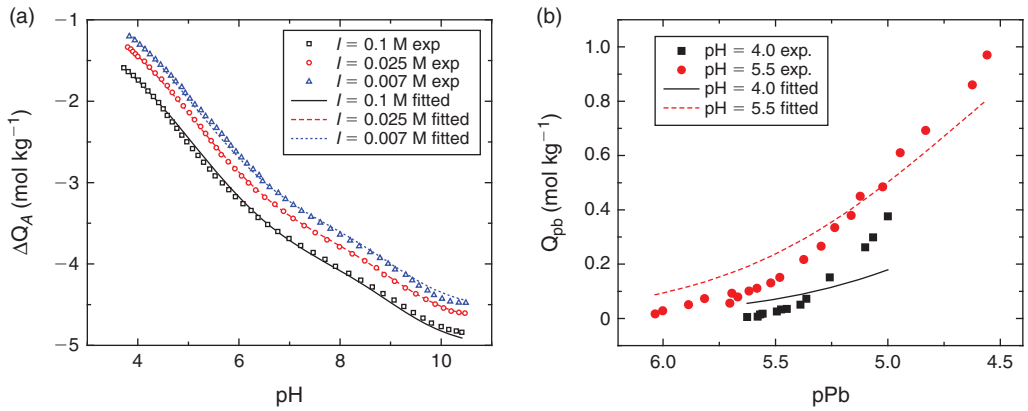

Fig. 1. (a) Acid–base titration curves of LHA in $NaClO_4$ at different *I*. (b) Titration curves of LHA with Pb^{II} at different pHs, *I* 0.1 M. Symbols: experimental; lines: fitting to the NICA-EPN model.

Table 1. Fitting parameters for LHA proton and Pb^{II} binding in the NICA-EPN model

Proton binding parameters											
Log K_{H1}	m_{H1}	q_1	Log K_{H2}	m_{H2}	q_2	Q_{max} (mol kg^{-1})	χ	v_2 (L mol^{-1})	g_f	b	Ref.
4.29	0.32	0.83	9.85	0.65	0.17	−5.57	0.79	4.8	0.28	—	This work[A]
3.54	0.78	0.60	8.0	0.26	0.40	−6.39	—	—	—	0.43	HH-03 (Milne et al. 2001)
3.22	0.52	0.58	8.0	0.52	0.42	−7.77	—	—	—	0.68	HH-10 (Milne et al. 2001)
Pb^{II} binding parameters											
Log $K_{Pb,1}$	$n_{Pb,1}$	p_1	Log $K_{Pb,2}$	$n_{Pb,2}$	p_2						
2.55	0.95	0.95	7.92	0.10	0.68						This work[B]
1.5	0.60	0.62	4.84	0.69	0.41						Generic values (Milne et al. 2003)

[A] $R^2 = 0.999$; RMSE = 0.040. [B] $R^2 = 0.911$; RMSE = 0.075.

those given by the IHSS, albeit determined by a different method (Ritchie and Perdue 2003). It should be noted that a high proportion of carboxylic over phenolic sites are found, as compared with other HS (Milne et al. 2001). The ND values for log K_{H1} are noticeably lower than those found here. It has been already observed that the ND parameters are lower than other model estimations (Matynia et al. 2010), albeit this has been partially corrected with optimised procedures (Lenoir et al. 2010). The difference between the two models has been attributed to an overestimation of electrostatic interactions by the ND model: computations of the electrostatic contribution to the free energy of binding show consistently higher results (in absolute value) for the ND model compared with EPN (Montenegro et al. 2014) thus consequently the opposite happens for the intrinsic contribution, resulting in lower log *K* values. The m_{H1} values are quite different between the two ND datasets. The HH-10 result is closer to the present one. In the case of log K_{H2} the ND reported values are assumed, not fitted, due to insufficient data (low pH range), so that comparison of the phenolic parameters is precluded.

Fig 1b shows the Pb-titration curves of LHA at two pH values, the lines are calculated from the fitting to the NICA-EPN model. The resulting parameters are presented in Table 1, compared with the generic (average) ND parameters reported by Milne et al. (2003). There is little agreement, as the Milne parameters are dominated by the purified peat humic acid (HA). The agreement between experimental data and fitted curves is reasonable at pH 5.5 but only fair at pH 4.0. It has been discussed elsewhere (Montenegro et al. 2014), that the NICA equation predicts parallel isotherms (in the log–log plot) at low metal concentrations for different pHs. The experimental curves, however, are not parallel here and so cannot be reproduced precisely by the NICA equation. This behaviour has been also observed in the interaction of Pb^{II} with other HS (Orsetti et al. 2013; Montenegro et al. 2014).

The NICA-EPN model predicts the Donnan potential (ψ_D) and the swelling parameter (φ_2) (the ratio of the volume of the dry HS to the full hydrated volume), which can be converted into the ratio of the hydrated humic particle mean radius (*r*) to the dry particle mean radius (r_0) (Eqn 5):

$$\frac{r}{r_0} = \frac{1}{\varphi_2^{1/3}} \tag{5}$$

The results obtained for ψ_D and r/r_0 of LHA as a function of pH are shown in Figs S1 and S2 (Supplementary Material). Relatively low changes are observed, compared with other HS as reported by Orsetti et al. (2010), especially for volume changes.

The speciation of bound H^+ between different sites, both external and internal, can also be obtained from the model results. From the general NICA-EPN expressions (Eqn S11, Supplementary Material) in the case of H^+ binding only, the fraction of protonated internal sites is given by Eqn 6:

$$\theta_{k,i} = \frac{\left(K_{H,k} a_{H^+}^{int}\right)^{m_{H,k}}}{1 + \left(K_{H,k} a_{H^+}^{int}\right)^{m_{H,k}}} \tag{6}$$

for $k = 1$ (carboxylic like) and $k = 2$ (phenolic like) sites; likewise, for external sites (Eqn 7):

$$\theta_{k,e} = \frac{\left(K_{\mathrm{H},k} a_{\mathrm{H}^+}\right)^{m_{\mathrm{H},k}}}{1 + \left(K_{\mathrm{H},k} a_{\mathrm{H}^+}^{\mathrm{int}}\right)^{m_{\mathrm{H},k}}} \tag{7}$$

whereas the fraction of anionic (unprotonated) sites is given by Eqn 8:

$$\theta_A = 1 - \theta_{1,i} - \theta_{1,e} - \theta_{2,i} - \theta_{2,e} \tag{8}$$

Fig. S3 (Supplementary Material) shows the LHA acid–base speciation. It is found that internal sites remain protonated in a wider pH range than external ones, due to the Donnan equilibrium-enhanced internal H^+ activity. It is observed also that below pH 6 the external sites are increasingly protonated and that at pH 2 ~90 % of the sites are protonated, and the humic charge is strongly decreased.

The speciation of Pb^{II} among HA sites can also be obtained from the NICA-EPN parameters by evaluating Eqn S11 (Supplementary Material). It is found (Fig. S4, Supplementary Material) that almost all Pb^{II} is bound to the carboxylic sites. In the presence of Pb, consequently, the proton speciation is only affected for the internal carboxylic sites (Fig. S5, Supplementary Material). This behaviour is mainly due to the Donnan effect on the divalent Pb^{2+} ions. Fig. S6 (Supplementary Material) shows the Donnan potential which is about −60 mV in the absence of Pb^{II} at pH 5 and decreases (in absolute value) to near −40 mV at pPb 4, and the resulting Boltzmann factor (Eqn S9, Supplementary Material) which ranges between ~95 and 20 in the pPb range of 6 to 4. Thus, the highly increased Pb^{II} activity in the gel fraction is responsible for the speciation observed. Consequently, protons are displaced from internal sites in the presence of Pb^{II}.

AFM observation of pH effect on humic particles

Fig. 2 shows typical pseudocolor AFM images of LHA deposited on mica sheets. Albeit these are ex-situ images, care was exercised to dry the samples gently in air, so as to avoid alterations to the particles. It is observed that in all cases relatively small particles are found, together with larger covered areas, which increase in size as pH decreases. These larger areas are clearly agglomerates, which are expected to be favoured by the lower humic charge in acidic media.

As it is well known, in AFM, height measurements (z axis) are more accurate than width/area measurements (x and y axes) for small particles so that in the following height results are analysed. Grain detection was performed by thresholding and filtering (details in Supplementary Material). The maximum height of each particle was taken. This set of the grain heights was used as the parameter for a statistical analysis. For this purpose a high number of images was acquired and processed, analysing over 570 particles at each pH.

Fig. 3 shows the particle height distribution, plotted as normalised total height (Eqn 3) as a function of individual height. This representation allows for better observation. Clearly, this figure reveals two ranges: a Gaussian-like mode at low heights and a more dispersed sequence of peaks for large heights. The lower part is attributable to individual particles whereas the rest of the peaks, which are reduced until almost vanishing at higher pHs, should be due to agglomerates. Thus the above results were analysed separately as individual

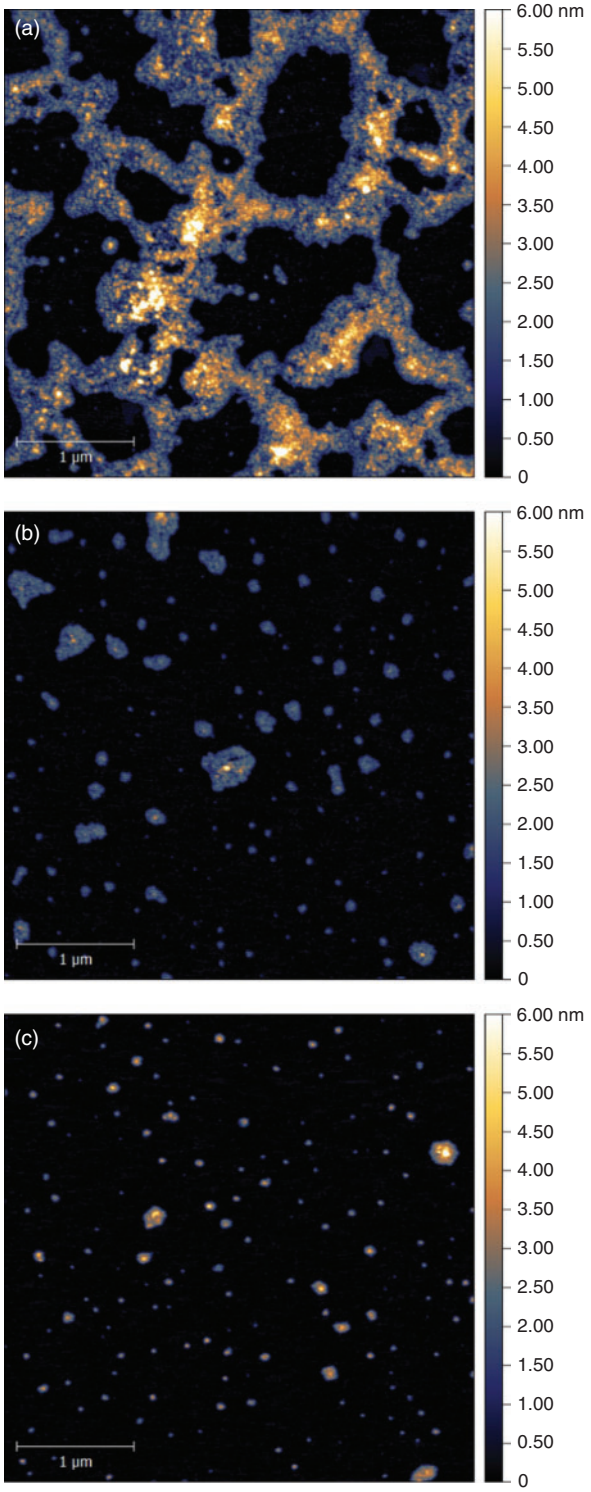

Fig. 2. Example AFM pseudocolour images of LHA sorbed on mica sheets, deposited at (a) pH 2.0, (b) pH 7.0 and (c) pH 11.0.

particles and agglomerates, filtering by the highest value in the particle volume distribution (2×10^4 nm^3) at pH 11.0 as the criterion for differentiation between individual particles and agglomerates.

Fig. 4 shows the individual particle height distribution for different pHs. A small increase in sizes is incipient at pH 8.0 and distinctly observed at pH 11.0. The distribution shape is approximately Gaussian. The h_N values as a function of pH are plotted

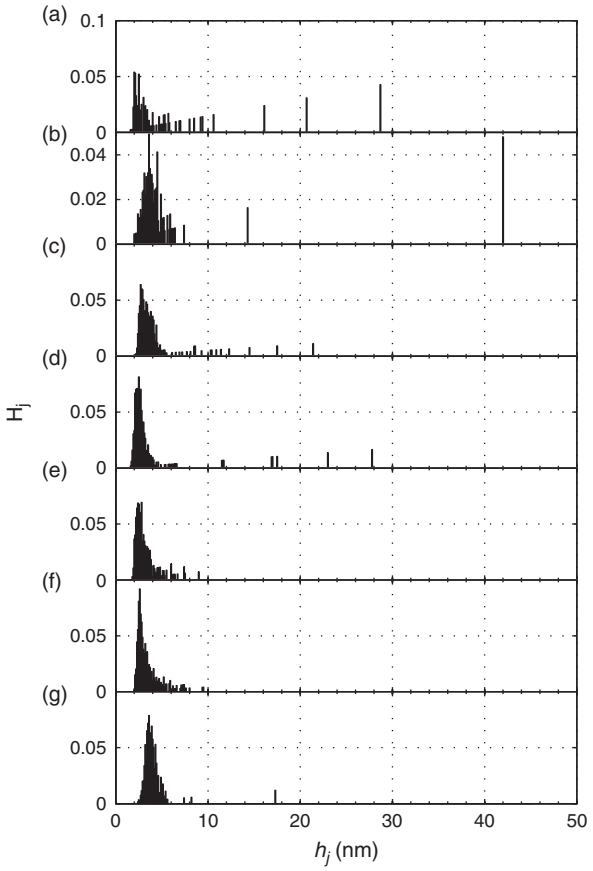

Fig. 3. Particle height distributions plotted as normalised total height as a function of height for different pH values: (a) 2.0, (b) 4.0, (c) 5.0, (d) 6.0, (e) 7.0, (f) 8.0 and (g) 11.0.

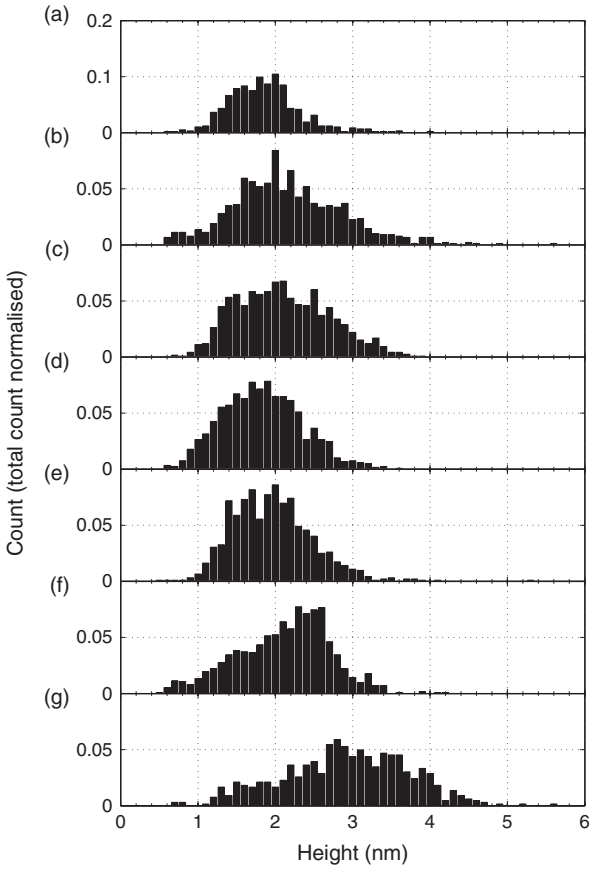

Fig. 4. Particle size distribution of individual particles at different pH values: (a) 2.0 (b) 4.0 (c) 5.0 (d) 6.0 (e) 7.0 (f) 8.0 and (g) 11.0.

in Fig. 5 (circles). Within experimental uncertainty, only a small change in size in the most alkaline medium is observed. This behaviour can be related to the small change in electrostatic Donnan potential resulting for this HA (see Fig. S1, Supplementary Material). Because the experiments were performed ex-situ, quantitative comparison with model calculations, which are based on parameters obtained from titration measurements, cannot be done. However, a qualitative comparison can be useful. In Fig. 5, the model prediction for r/r_0 at an ionic strength of 0.01 M, taking as reference the radius at pH 2.0, is plotted as a dashed line. This prediction is based on the parameter values obtained from titration curves only. The model predicts a small size change, which is consistent with the experimental results within experimental error. Albeit the model could be fitted including the size results for better parameter adjustment, in this case clearly this is not reasonable since size measurements were performed ex-situ. For the same reasons, model agreement cannot be concluded; however, Fig. 5 clearly suggests that the NICA-EPN model is consistent with the experimental behaviour.

Fig. 6 shows the dispersity as a function of pH. An increase at pH $<$ 5 is clearly observed, reflecting the agglomeration observed in the images. As it has been previously discussed by several authors (Balnois et al. 1999; Duval et al. 2005; da Costa Saab et al. 2010;), at acidic pH the protonation of anionic sites leads to both a decrease in negative charge, thus decreased repulsion, and an increase in OH groups capable of hydrogen binding different humic particles. The total interaction energy

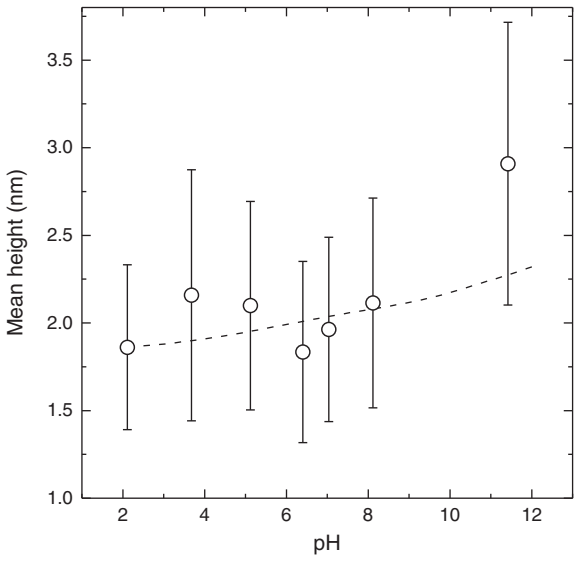

Fig. 5. Symbols: experimental mean (number-average) particle height; dashed line: NICA-EPN predicted size increase (referred to pH 2), as a function of pH.

between particles can be written here as Eqn 9 (Israelachvili 2010, Chapter 14):

$$W = W_{\mathrm{VdW}} + W_{\mathrm{chem}} + W_{\mathrm{el}} \qquad (9)$$

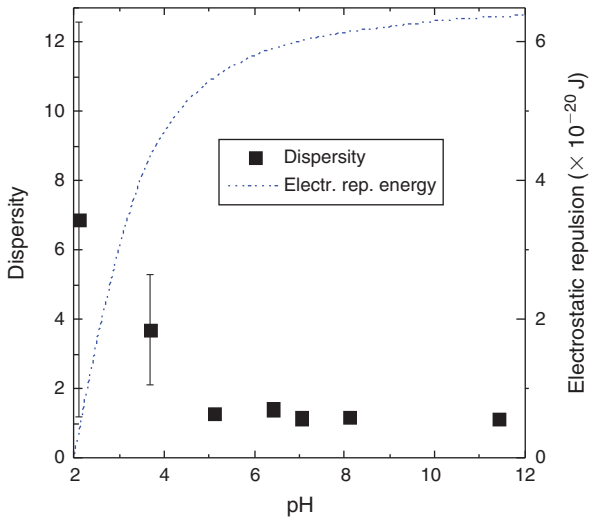

Fig. 6. Dispersity of agglomerates (symbols) and particle–particle electrostatic repulsion energy (dotted line) as a function of pH.

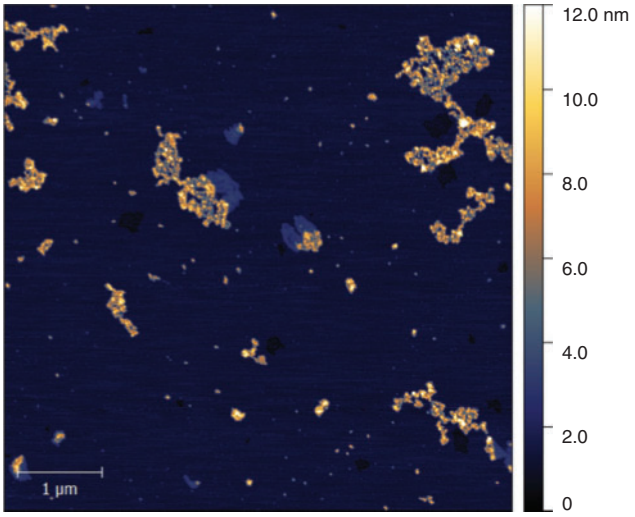

Fig. 7. AFM pseudocolour image of LHA particles adsorbed on muscovite in the presence of 25 µm (total concentration) Pb^{II}, in 0.1 M $NaClO_4$.

where W_{VdW} is the van der Waals interaction energy, W_{chem} is the 'chemical bond' interaction, here representing hydrogen bonds, and W_{el} is the electrostatic contribution. The first contribution is attractive and largely independent of pH. For W_{chem} it is difficult to derive an expression, however it is an attractive, short range interaction, and is expected to be dependent on the number of H-bond capable groups, which in humics are mainly OH groups. As noted above (see Fig. S3, Supplementary Material), the external carboxylate groups are increasingly protonated below pH 6, thus W_{chem} should increase as the pH decreases below that value.

To estimate W_{el}, which is expected to be repulsive due to the negative charge, here we will consider the humic particles as approximately spherical, and use the classic Derjaguin expression for identical spheres at short distance (lower than the particle radius), in an 1:1 electrolyte medium (Eqn 10) (Israelachvili 2010, Chapter 14):

$$W_{el}(D) = 32r\pi\varepsilon\varepsilon_0\left(\frac{RT}{F}\right)^2 \tanh^2\left(\frac{zF\psi}{4RT}\right)e^{-\kappa D} \qquad (10)$$

where r is the sphere radius, ε is the relative dielectric constant, ε_0 the vacuum permittivity, ψ the surface potential, κ the Debye inverse length, and D the interparticle distance. We take here r as the NICA-EPN results of Fig. 5 (in the order of 2 nm), D as the contact distance, which is generally estimated as $D_0 = 0.165$ nm, a value which has been found to be consistent with the surface energy of many substances (Israelachvili 2010, Chapter 13), and ψ as the NICA-EPN predicted Donnan potential. The result of Eqn 10 is plotted in Fig. 6, dotted line, showing a marked decrease below pH 6. Thus the agglomeration, as measured by the dispersity, can be attributed to the combined effect of the decrease of electrostatic repulsion and an increase of hydrogen binding capability of LHA particles, which leads to an overcoming of repulsion barriers allowing aggregation. It should be noted that this is a very approximate estimation, due to the heterogeneous nature of HS. A more exact treatment would require detailed knowledge of LHA molecular structure, which is little known and is beyond the scope of the present work. Another observation, comparing the experimental results of Figs 5 and 6, is that there is no apparent relationship between the dispersity and the individual particle size; that is, the changes in dispersity are due to aggregation.

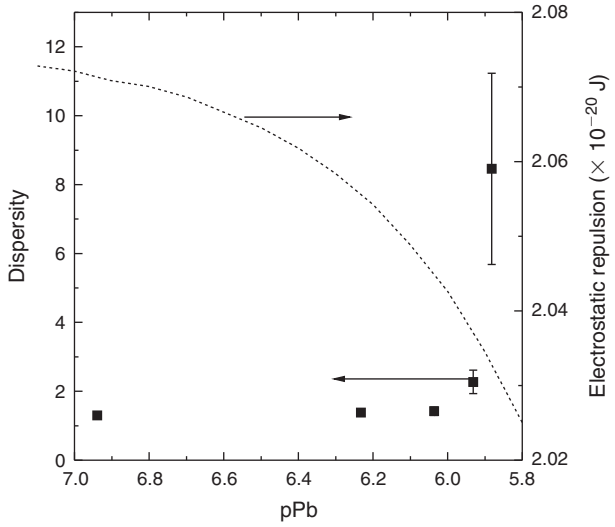

Fig. 8. Symbols: dispersity of agglomerates observed in the presence of Pb^{II} as a function of free Pb^{2+} activity, estimated with the NICA-EPN model (pH 5.0, 0.01 M $NaClO_4$). Dotted line: particle–particle electrostatic repulsion energy as a function of Pb^{2+} activity, as predicted by the NICA-EPN model.

AFM observation of Pb^{II} binding to LHA humic particles

In the presence of Pb^{II}, the size and shape of the agglomerates changes, resulting in structures like those shown in Fig. 7. These structures grow rapidly as the Pb concentration increases. This evolution was also evaluated through the dispersity, the results being presented in Fig. 8 as a function of free Pb^{2+} activity (a_{Pb}) plotted as pPb = $-\log a_{Pb}$ (0–50 µM total Pb at pH 5.0), as estimated with the NICA-EPN model as follows. Using the parameters detailed in Table 1, a Pb binding curve at pH 5.0 and I 0.1 M was computed for pPb values between 7.0 and 5.8. From the results for Q_{Pb} and the pPb data the total Pb concentration was obtained and, finally, the pPb values corresponding to the measurements of Fig. 8 were interpolated. A steep rise of

dispersity is observed at pPb $\approx$ 5.9. In the concentration range shown the model predicts an almost constant electrostatic potential, as shown in Fig. 8 (also obtained with Eqn 10), and humic particle size, thus this effect should not be the cause for agglomeration. Metal cations are able to bridge humic molecules together, a fact which in the case of Pb has been noted elsewhere (Orsetti et al. 2013) so that the complexation of Pb^{II} cations with humic molecules is consistent with the aggregation observed. Similar results were observed for other HS and cations (Guo and Ma 2006; Liu et al. 2001; Plaschke et al. 2002). Due to lack of information, at present a quantitative analysis cannot be performed. However, a qualitative interpretation can be done as follows. We consider a general reaction for agglomerates forming between HA and Pb^{II} as Eqn 11:

$$N\mathrm{HA} + M\mathrm{Pb}^{\mathrm{II}} \rightleftharpoons (\mathrm{HA})_N\mathrm{Pb}_M \tag{11}$$

The equilibrium condition can be written as Eqn 12:

$$N\mu_{\mathrm{HA}} + M\mu_{\mathrm{Pb}} = \mu_{\mathrm{Ag}}(N, M) \tag{12}$$

where Ag stands for aggregate.

We will estimate the aggregate chemical potential by applying the thermodynamic theory of self-aggregation (Israelachvili 2010, Chapter 19). For similar molecules forming aggregates, the chemical potential per HA molecule in an aggregate containing N molecules can be written as Eqn 13:

$$\mu_{\mathrm{HA}}(N) = \mu^0_{\mathrm{HA},N} + \frac{kT}{N}\ln\left(\frac{x_N}{N}\right) \tag{13}$$

where x_N is the mole fraction of molecules forming aggregates which contain N HA molecules, k is Boltzmann's constant and, for a spherical-like aggregate,

$$\mu^0_{\mathrm{HA},N} = \mu^\infty_{\mathrm{HA}} + \frac{\alpha kT}{N^{1/3}} \tag{14}$$

where $\mu^\infty{}_{\mathrm{HA}}$ is the average chemical potential of an HA molecule in an infinite aggregate and the second term accounts for the energy of surface unbound molecules, αkT being the average molecule binding energy in the aggregate relative to isolated solution molecules. We assume that Eqns 13 and 14 hold for the HA in the HA-Pb aggregate, and the same functional form holds for the metal cations (Eqns 15, 16):

$$\mu_{\mathrm{Pb}}(M) = \mu^0_{\mathrm{Pb},M} + \frac{kT}{M}\ln\left(\frac{x_M}{M}\right) \tag{15}$$

$$\mu^0_{\mathrm{Pb},M} = \mu^\infty_{\mathrm{Pb}} + \frac{\beta kT}{M^{1/3}} \tag{16}$$

where x_M is the mole fraction of Pb^{II} cations in an aggregate containing M cations and βkT the average Pb^{II} binding energy in the aggregate relative to isolated solution ions. In Eqns 14 and 16, $\mu^\infty{}_{\mathrm{HA}}$ and $\mu^\infty{}_{\mathrm{Pb}}$ are assumed to include the average HA-Pb interaction energy per HA molecule and Pb^{II} ion, respectively. With Eqns 13–16 the aggregate chemical potential can be written as Eqn 17:

$$\mu_{\mathrm{Ag}}(N, M) = N\mu_{\mathrm{HA}}(N) + M\mu_{\mathrm{Pb}}(M) \tag{17}$$

In a previous study (Orsetti et al. 2013) it was found from fluorescence measurements that the results can be interpreted through the formation of aggregates having a fixed average number (n) of Pb^{II} ions per HA molecule (with $1 \le n \le 2$), thus Eqn 18 will be assumed:

$$M = nN \tag{18}$$

Note that Eqn 18 implies that $x_M = nx_N$. Introducing Eqns 13–18 into Eqn 12, and writing for the chemical potentials in solution $\mu_J = \mu^0_{J,\mathrm{aq}} + kT\ln a_J$ (where aq stands for aqueous) gives Eqn 19:

$$\begin{aligned} &N[-\Delta\mu_{\mathrm{HA}} - n\Delta\mu_{\mathrm{Pb}} + kT(\ln a_{\mathrm{HA}} + n\ln a_{\mathrm{Pb}})] \\ &= \left(\alpha + n^{2/3}\beta\right)kTN^{2/3} + 2kT\ln\left(\frac{x_N}{N}\right) \end{aligned} \tag{19}$$

where

$$\Delta\mu_J = \mu^\infty_J - \mu^0_{J,\mathrm{aq}} \tag{20}$$

Introducing Eqn 21

$$\ln K = \frac{-\Delta\mu_{\mathrm{HA}} - n\Delta\mu_{\mathrm{Pb}}}{kT} \tag{21}$$

and Eqn 22

$$\ln A = \ln a_{\mathrm{HA}} + n\ln a_{\mathrm{Pb}} \tag{22}$$

Eqn 23 is determined for the mole fraction of HA molecules forming aggregates of N molecules:

$$x_N = N(KA)^{N/2}e^{-\delta N^{1/3}} \tag{23}$$

with $\delta = \alpha + n^{2/3}\beta$. Fig. 9 shows a schematic representation of x_N as a function of N as in Eqn 23 for different KA values, where it can be seen that for increasing KA (here, increasing Pb^{II} activity) the width of the distribution of x_N increases, which implies increasing dispersity, in qualitative agreement with the results of Fig. 8. It can be verified that for $KA > 1$, the x_N values

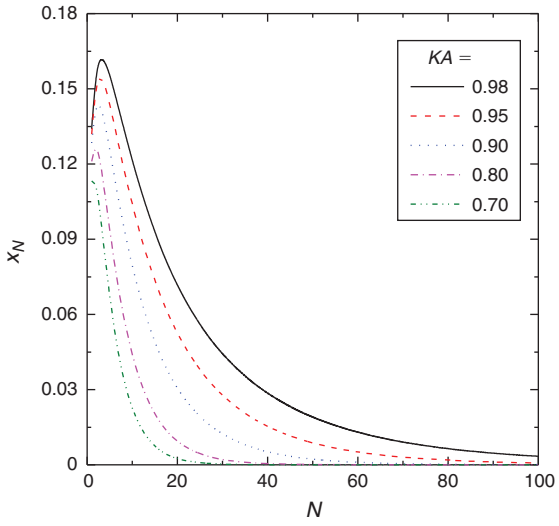

Fig. 9. Mole fraction of HA molecules forming aggregates of N molecules, as a function of N, for different values of the product KA; $\delta = 2.0$. See text for details.

diverge, thus $KA = 1$ can be regarded as the onset of precipitation. These considerations support the assumption that HA agglomeration in the presence of Pb^{II} is due to the binding interaction between the HA and the metal. Further studies will be conducted on this aspect.

Conclusions

The aggregation behaviour of a humic substance is analysed and found to correlate with chemical binding: corresponding to hydrogen bonding in acidic media, due to full protonation of carboxylate sites, and due to metal cation bridging, with Pb^{II} in the present study. Electrostatic repulsion, inhibiting close association in alkaline media, also plays a role in the absence of metal cations. The comparison between results of ex-situ AFM measurements and predictions of the NICA-EPN model suggest consistency between theory and experiment.

Supplementary Material

A brief description of the NICA-EPN theory, experimental details including image processing procedures, supplementary results and references are available on the Journal's website.

Conflicts of interest

The authors declare no conflicts of interest.

Acknowledgements

The authors gratefully acknowledge financial support from the Universidad de Buenos Aires (UBACYT 20020130100035BA), the Consejo Nacional de Investigaciones Científicas y Técnicas (CONICET, PIP F57269) and the Agencia Nacional de Promoción Científica y Tecnológica (grant PICT 2014-2289). F. d. R. C. thanks the DAAD for a fellowship and Prof. S. Haderlein, Universität Tübingen for a stay in his group. F. V. M. and L. L. are members of the Carrera del Investigador Científico of CONICET. F. d. R. C., S. O. and F. V. M. are members of the International Humic Substances Society.

References

Baigorri R, Fuentes M, González-Gaitano G, García-Mina JM (2007). Analysis of molecular aggregation in humic substances in solution. *Colloids and Surfaces A: Physicochemical and Engineering Aspects* **302**, 301–306. doi:10.1016/J.COLSURFA.2007.02.048

Baldssock JA, Nelson PN (1999). Soil organic matter. In 'Handbook of soil science'. (Ed. ML Sumner) pp. B75–B84. (CRC: Boca Raton, FL)

Balnois E, Wilkinson KJ (2002). Sample preparation techniques for the observation of environmental biopolymers by atomic force microscopy. *Colloids and Surfaces A: Physicochemical and Engineering Aspects* **207**, 229–242. doi:10.1016/S0927-7757(02)00136-X

Balnois E, Wilkinson KJ, Lead JR, Buffle J (1999). Atomic force microscopy of humic substances: effects of pH and ionic strength. *Environmental Science & Technology* **33**, 3911–3917. doi:10.1021/ES990365N

Benedetti MF, Milne CJ, Kinniburgh DG, Van Riemsdijk WH, Koopal LK (1995). Metal ion binding to humic substances: application of the non-ideal competitive adsorption model. *Environmental Science & Technology* **29**, 446–457. doi:10.1021/ES00002A022

Buffle J, Altmann RS, Filella M, Tessier A (1990). Complexation by natural heterogeneous compounds: site occupation distribution functions, a normalized description of metal complexation. *Geochimica et Cosmochimica Acta* **54**, 1535–1553. doi:10.1016/0016-7037(90)90389-3

Chen C, Wang X, Jiang H, Hu W (2007). Direct observation of macromolecular structures of humic acid by AFM and SEM. *Colloids and Surfaces A: Physicochemical and Engineering Aspects* **302**, 121–125. doi:10.1016/J.COLSURFA.2007.02.014

Chilom G, Rice JA (2009). Structural organization of humic acid in the solid state. *Langmuir* **25**, 9012–9015. doi:10.1021/LA900750Z

da Costa Saab S, Carvalho ER, Bernardes Filho R, de Moura MR, Martin-Neto L, Mattoso LHC (2010). pH effect in aquatic fulvic acid from a Brazilian river. *Journal of the Brazilian Chemical Society* **21**, 1490–1496. doi:10.1590/S0103-50532010000800012l

David C, Mongin S, Rey-Castro C, Galceran J, Companys E, Garcés JL, Salvador J, Puy J, Cecilia J, Lodeiro P, Mas F (2010). Competition effects in cation binding to humic acid: conditional affinity spectra for fixed total metal concentration conditions. *Geochimica et Cosmochimica Acta* **74**, 5216–5227. doi:10.1016/J.GCA.2010.06.023

Duval JFL, Wilkinson KJ, Van Leeuwen HP, Buffle J (2005). Humic substances are soft and permeable: evidence from their electrophoretic mobilities. *Environmental Science & Technology* **39**, 6435–6445. doi:10.1021/ES050082X

García R, Pérez R (2002). Dynamic atomic force microscopy methods. *Surface Science Reports* **47**, 197–301. doi:10.1016/S0167-5729(02)00077-8

Goldberg S (2005). Equations and models describing adsorption processes in soils. In 'Chemical processes in soils'. (Eds MA Tabatabai, DL Sparks) pp. 489–518. (Soil Science Society of America: Madison, WI)

Gorham JM, Wnuk JD, Shin M, Fairbrother H (2007). Adsorption of natural organic matter onto carbonaceous surfaces: atomic force microscopy study. *Environmental Science & Technology* **41**, 1238–1244. doi:10.1021/ES061793D

Guo J, Ma J (2006). AFM study on the sorbed NOM and its fractions isolated from River Songhua. *Water Research* **40**, 1975–1984. doi:10.1016/J.WATRES.2006.03.012

Gustafsson JP, Pechova P, Berggren D (2003). Modeling metal binding to soils: the role of natural organic matter. *Environmental Science & Technology* **37**, 2767–2774. doi:10.1021/ES026249T

Israelachvili JN (2010). 'Intermolecular and surface forces, 3rd edn.' (Academic Press: Amsterdam)

Kinniburgh DG, Milne CJ, Benedetti MF, Pinheiro JP, Filius J, Koopal LK, Van Riemsdijk WH (1996). Metal ion binding by humic acid: application of the NICA-Donnan model. *Environmental Science & Technology* **30**, 1687–1698. doi:10.1021/ES950695H

Kinniburgh DG, Van Riemsdijk WH, Koopal LK, Borkovec M, Benedetti MF, Avena MJ (1999). Ion binding to natural organic matter: competition, heterogeneity, stoichiometry and thermodynamic consistency. *Colloids and Surfaces A: Physicochemical and Engineering Aspects* **151**, 147–166. doi:10.1016/S0927-7757(98)00637-2

Lenoir T, Matynia A, Manceau A (2010). Convergence-optimized procedure for applying the NICA–Donnan model to potentiometric titrations of humic substances. *Environmental Science & Technology* **44**, 6221–6227. doi:10.1021/ES1015313

Liu C, Frenkel AI, Vairavamurthy A, Huang PM (2001). Sorption of cadmium on humic acid: mechanistic and kinetic studies with atomic force microscopy and X-ray absorption fine structure spectroscopy. *Canadian Journal of Soil Science* **81**, 337–348. doi:10.4141/S00-070

Matynia A, Lenoir T, Causse B, Spadini L, Jacquet T, Manceau A (2010). Semi-empirical proton binding constants for natural organic matter. *Geochimica et Cosmochimica Acta* **74**, 1836–1851. doi:10.1016/J.GCA.2009.12.022

Milne CJ, Kinniburgh DG, De Wit JCM, Van Riemsdijk WH, Koopal LK (1995). Analysis of proton binding by a peat humic acid using a simple electrostatic model. *Geochimica et Cosmochimica Acta* **59**, 1101–1112. doi:10.1016/0016-7037(95)00027-W

Milne CJ, Kinniburgh DG, Tipping E (2001). Generic NICA–Donnan model parameters for proton binding by humic substances. *Environmental Science & Technology* **35**, 2049–2059. doi:10.1021/ES000123J

Milne CJ, Kinniburgh DG, van Riemsdijk WH, Tipping E (2003). Generic NICA–Donnan model parameters for metal-ion binding by humic substances. *Environmental Science & Technology* **37**, 958–971. doi:10.1021/ES0258879

Molina FV (2013). 'Soil colloids: properties and ion binding.' (CRC Press: Boca Raton, FL).

Montenegro AC, Orsetti S, Molina FV (2014). Modelling proton and metal binding to humic substances with the NICA-EPN model. *Environmental Chemistry* **11**, 318–332. doi:10.1071/EN13214

Orsetti S, Andrade EM, Molina FV (2010). Modeling ion binding to humic substances: elastic polyelectrolyte network model. *Langmuir* **26**, 3134–3144. doi:10.1021/LA903086S

Orsetti S, Marco-Brown JL, Andrade EM, Molina FV (2013). Pb(II) binding to humic substances: an equilibrium and spectroscopic study. *Environmental Science & Technology* **47**, 8325–8333. doi:10.1021/ES400999Q

Plaschke M, Rothe J, Schäfer T, Denecke MA, Dardenne K, Pompe S, Heise K-H (2002). Combined AFM and STXM in situ study of the influence of Eu(III) on the agglomeration of humic acid. *Colloids and Surfaces A: Physicochemical and Engineering Aspects* **197**, 245–256. doi:10.1016/S0927-7757(01)00901-3

Puy J, Galceran J, Huidobro C, Companys E, Samper N, Garcés JL, Mas F (2008). Conditional affinity spectra of Pb2+-humic acid complexation from data obtained with AGNES. *Environmental Science & Technology* **42**, 9289–9295. doi:10.1021/ES8021123

Puy J, Huidobro C, David C, Rey-Castro C, Salvador J, Companys E, Garcés JL, Galceran J, Cecília J, Mas F (2009). Conditional affinity spectra underlying NICA isotherm. *Colloids and Surfaces A: Physicochemical and Engineering Aspects* **347**, 156–166. doi:10.1016/J.COLSURFA.2009.03.053

Ritchie JD, Perdue EM (2003). Proton-binding study of standard and reference fulvic acids, humic acids, and natural organic matter. *Geochimica et Cosmochimica Acta* **67**, 85–96. doi:10.1016/S0016-7037(02)01044-X

Senesi N, Loffredo E (1998). The chemistry of soil organic matter. In 'Soil physical chemistry'. (Ed. DL Sparks) pp. 239–370. (CRC Press: Boca Raton, FL)

Simpson AJ, Kingery WL, Hayes MH, Spraul M, Humpfer E, Dvortsak P, Kerssebaum R, Godejohann M, Hofmann M (2002). Molecular structures and associations of humic substances in the terrestrial environment. *Naturwissenschaften* **89**, 84–88. doi:10.1007/S00114-001-0293-8

Sutton R, Sposito G (2005). Molecular structure in soil humic substances: the new view. *Environmental Science & Technology* **39**, 9009–9015. doi:10.1021/ES050778Q

Tipping E (1998). Humic ion-binding model VI: an improved description of the interactions of protons and metal ions with humic substances. *Aquatic Geochemistry* **4**, 3–47. doi:10.1023/A:1009627214459

Wershaw RL (2004). Evaluation of conceptual models of natural organic matter (humus) from a consideration of the chemical and biochemical processes of humification (Scientific Investigations Report No. 2004-5121). USGS, Denver, CO.

Zhong Q, Inniss D, Kjoller K, Elings VB (1993). Fractured polymer/silica fiber surface studied by tapping mode atomic force microscopy. *Surface Science Letters* **290**, L688–L692. doi:10.1016/0167-2584(93)90906-Y

Handling Editor: Kevin Wilkinson